JOURNAL OF APPLIED ELECTROCHEMISTRY 8 (1978) 145–160

Corrosion of nickel in sodium sulphate -sodium chloride melts. Part I.

C. A. C. SEQUEIRA, M. G. HOCKING

Metallurgy and Materials Science Department, Imperial College, London SW7, UK

Received 31 May 1977

The corrosion behaviour of Ni in molten Na_2SO_4, NaCl, and in mixtures of these two salts, at 900° C, in laboratory air and under $O_2 + SO_2/SO_3$ atmospheres has been examined by electrochemical curves and topochemical analysis of corrosion products.

Ni passivity in pure Na_2SO_4 was observed under potentiodynamic and potentiometric conditions, the passive film corresponding to NiO. Passivity was not so easy to achieve in chloride melts as in sulphate alone, but once a thick oxide film forms on the specimen, the Cl^- addition is accompanied by an increase in the film stability. The inhibiting role of NaCl on Ni in the passive–transpassive area was also evidenced. In opposition, halide additions (especially those up to 25%) increased the dissolution current densities of Ni in the active region. These higher dissolution rates are represented by the equation

$$Ni_3S_2 + 4NaCl + 1/2\,O_2 = 2NiCl_2 + 2Na_2S + NiO$$

which is also suggested as a critical factor in the Ni passivation.

The passive capability found for Ni in Na_2SO_4/NaCl melts, in air, is destroyed by SO_3 atmospheres. This corrosion-stimulation is due to the SO_3 role in promoting reactions such as

$$NiS + 3O^{2-} = Ni^{2+} + SO_3 + 8e$$

which would be potential-determining at the Ni surface until Ni^{2+} precipitates or the conjugate oxygen cathodic reduction process takes place. Microprobe analysis also evidenced S penetration which might be the reason for the Ni embrittlement.

The polarization curves for Ni in pure NaCl showed the lack of a passive region; occurrence of extensive intergranular attack was also indicated by metallographic observation. The observed dissolution must occur at the expense of the Ni interactions with the species which intervene in the reaction equilibrium between O_2 and molten NaCl (O_2, Cl^-, Cl_2 and O^{2-}) as well as with the Na^+ cations, as has been discussed elsewhere. Its self-sustaining nature is enhanced by the continuous reduction of the nickel ion content of the melt by $NiCl_2$ evaporation.

1. Introduction

It is broadly recognized [1] that sodium chloride and sulphate form deposits (liquid at high temperature) which cause corrosion of gas turbine superalloys. Therefore, it was felt that important information regarding corrosion of the various superalloys can be obtained by means of an electrochemical analysis. Moreover, preliminary experiments in molten Na_2SO_4–NaCl mixtures have shown that it is possible to study the electrochemical behaviour of alloys by recording polarization curves, as has been done with great success in aqueous solutions. These electrochemical techniques have recently been employed by Arvia *et al.* [2, 3], Baudo *et al.* [4], Casino *et al.* [5], Kazantsev *et al.* [6], Pizzini and Agace [7] and others, in electrochemical investigations of the corrosion of metallic materials in molten media. Electrochemical studies in molten Na_2SO_4, NaCl, and Na_2SO_4/NaCl mixtures for the Ni-based alloys have rarely been taken up [8, 9]. A systematic research on Ni alloy electrodes in these melts by the potentiostatic techniques would allow an

understanding of the complex corrosion process involved and a comparison of corrosion resistance of different alloys by a quick and simple method, and so experiments began with the simplest system: pure Ni in fused Na_2SO_4, NaCl, and mixtures of these two salts, at 900° C. For this system, no similar studies have been reported.

The potentiostatic polarization may be divided into two types: potential sweep and potential step. At first sight, it might appear that the second method is to be preferred, since in theory it allows a steady state to be achieved between successive potential changes. However, studies in aqueous systems have shown that attainment of the steady state usually requires extremely long time intervals between measurements [10, 11] and, in addition, reproducibility between different specimens from the same metal or alloy is generally poor [12]. It has also been found by Greene and Leonard [12] that the potential step method is susceptible to timing errors associated with manual adjustment of the potentiostat, and for this reason (and the reasons above which might appear also in fused systems) the automatic potential sweep method (or potentiodynamic polarization technique) was selected for the present work.

The majority of the tests were conducted in laboratory air and under 1 atm oxygen and 5×10^{-5} atm SO_3 ($P_{SO_2} + P_{SO_3} \simeq 19{\cdot}3 \times 10^{-5}$ atm). These partial pressures were chosen to simulate the equilibrium partial pressures of these gases at the metal surface in a gas turbine operating at a high total pressure (~ 8 atm). Further tests in pure Na_2SO_4 under higher SO_3 partial pressures were carried out to get a better picture of the effect of the SO_3 which seems to be the principal oxidizing agent in molten sulphate environments [13].

Following the potentiodynamic series of experiments, it became clear that the active–passive transition present in several of the polarization curves was of importance, and the nature and stability of the passive film on Ni were studied by means of potential decay curves. Pure molten Na_2SO_4 and a molten mixture of Na_2SO_4–15% NaCl at 900° C, in air, were used.

Then it was decided to study the dependence of the open-circuit electrode potentials of nickel in Na_2SO_4–NaCl melts on time, melt composition, and the SO_3 atmosphere above the electrolyte. The information provided is useful, especially if the measurements are regarded as 'tests of orientation' which substantiate the conclusions taken from the potentiokinetic studies and serve as a tool in their interpretation.

Particular experiments have been concerned to determine the role of NaCl on Ni in the transpassive area. Also complementary topochemical studies were included to examine the corrosion reaction products.

2. Materials and Experimental Procedures

Analar chemicals and 1/2 mm Specpure Ni sheet were used. Low SO_2 atmospheres were obtained by passing O_2 over heated $CoSO_4$ and the resultant gas was analysed [14]. With all $SO_2 + O_2$ mixtures a Pt catalyst was used over the melt [15, 16]. Conventional Kanthal furnaces were used. A motorised Amel 551 potentiostat and electrometers were used for the electrochemical measurements. Degussit alumina crucibles of 160 ml capacity, containing 60 ml of melt, or Pt crucibles containing 30 ml of melt, were used, after cleaning. Square Ni electrodes of area 1 cm^2 were polished to Oakey's 4/0, spot welded to thin Pt wires, washed and degreased. Each electrode was placed in the melt after the salt had melted at 900° C. The counterelectrode was 1 cm^2 of Pt foil. The reference electrode is shown in Fig. 2 and its potential is the same whether evacuated or merely closed at the top by a pvc bulb through which the wire passes; closing is essential to prevent SO_3 escape from Ag_2SO_4 ($P_{SO_3} = 0{\cdot}012$ atm at 900° C). Reference electrodes are best stored at a red heat; long cooling times to ambient are necessary to prevent cracking. Against a Au wire electrode at 900° C, an 'ideal' Fig. 2 reference electrode has a potential of −160 mV. All measured potentials in this paper are given with respect to the Fig. 2 reference electrode. It is essential to pour sodium sulphate melts out hot, using tongs, to avoid contracting freezing melt pulling in the crucible walls. Bubbling nitrogen through melts to dry them [18] and remove OH^- ions [17] was investigated by recording *V–I* curves before and after, but the curves were essentially the same, not showing residual current or excursions due to dissolved impurities.

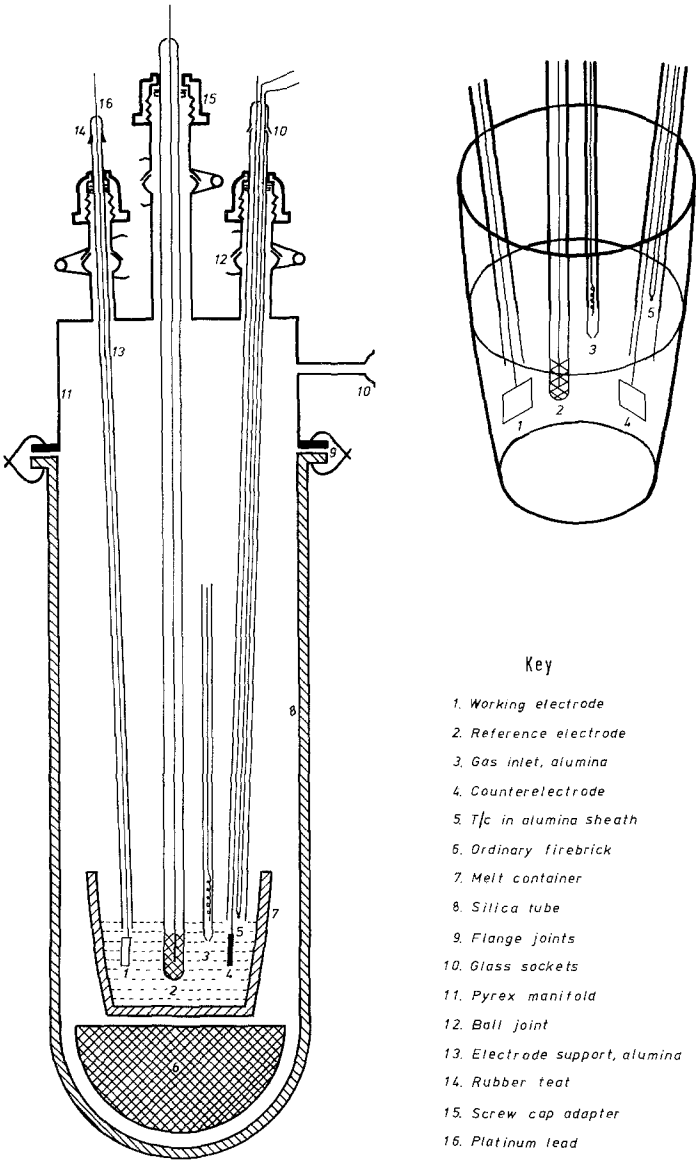

Key

1. Working electrode
2. Reference electrode
3. Gas inlet, alumina
4. Counterelectrode
5. T/c in alumina sheath
6. Ordinary firebrick
7. Melt container
8. Silica tube
9. Flange joints
10. Glass sockets
11. Pyrex manifold
12. Ball joint
13. Electrode support, alumina
14. Rubber teat
15. Screw cap adapter
16. Platinum lead

Fig. 1. High temperature assembly.

For the tests under 5×10^{-5} atm SO_3, 3 h was allowed for equilibration and small NaCl additions were made just before specimen insertion to make up for the NaCl vaporization loss (determined in separate experiments).

The nickel electrode was anodically polarized (for the V–I sweeps) when the maximum negative potential was reached, i.e. at about 5 min after insertion.

All experiments were performed with fresh electrolytes and specimens; representative experiments were done in duplicate or triplicate for reproducibility.

Further details of experimental techniques and materials are available in [19].

A brief study of the effect of varying the rate of polarization showed that the most meaningful curves are those obtained at traverse rates between 17 and 51 mV min^{-1} (approx.), and then a 25·5 mV min^{-1} scanning rate was selected for all potentiokinetic experiments on Ni which allowed completion of a single experiment in about 3 h.

In the potentiodynamic polarization experiments carried out in Na_2SO_4–NaCl melts, in air, it was found that the dissolution current density

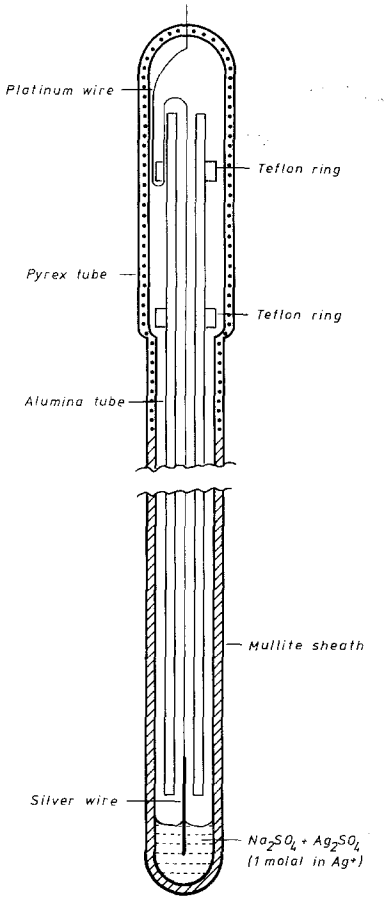

Fig. 2. Reference electrode.

for the anodic polarization of nickel in the overpassive region is lower in chloride melts than in sulphate alone. In addition the beginning of the transpassive region in chloride melts (especially those in the range 0 to 15% NaCl) shifts in the anodic direction (see Fig. 15). To confirm these results the following procedure was adopted. The test electrode was polarized in an aerated sulphate melt and taken into the overpassive (or transpassive) region in the absence of chloride ions. It was held at a potential in this area for 1 h, and then the current–time curves (at these potentials) were measured in the presence and absence of chloride ions.

3. Results and Discussion

3.1. *General*

A schematic diagram of a typical potentiodynamic polarization curve for an anodically polarized metal in a Na_2SO_4-containing environment is shown in Fig. 3 to assist in the later discussion of polarization curves. The symbols shown in the figure indicate critical potentials, a potential range and current densities that will be used throughout the paper. Curve E_sE_A represents an 'active' reaction of the type

$$M + xNa_2SO_4 \rightarrow M^{z+}(Na_2SO_4)_x + ze \quad (1)$$

and E_A is the potential where the formation of an oxide becomes thermodynamically possible, by, for example,

$$M + Na_2SO_4 \rightarrow MO + SO_3 + 2Na^+ + 2e.$$

Above E_A dissolution and oxide formation will occur so that the metal surface is not covered completely with an oxide film. At E_{pp}, the primary passive potential (or potential at which a sharp change in the slope of the E–i relationship occurs), the rate of film growth and the rate of dissolution become equal and $i = i_c$. At higher potentials the rate of film growth exceeds that of dissolution and the surface becomes almost completely filmed with an oxide with a consequent decrease in current, $E_{pp}E_p$.

Complete coverage occurs above E_p, the passivation potential, and the rate of the process is then determined by the rate of dissolution of the protective film. At E_t* the scarcely soluble passivating oxide is anodically oxidized to a soluble substance and/or disruption of the oxide film occurs by any factor associated with the metal or the electrolyte which increases the oxide solubility or ionic conductivity, etc. Above E_t, a further possibility is the oxidation of the ionic entities in the melt (e.g., sulphate ions, chloride ions, oxide ions) which will proceed readily at the film–melt interface if the film has a high electronic conductivity (and until the process becomes limited by mass-transfer in the electrolyte). In the reverse scan, below the repassivation potential, E_{rp}, the metal becomes protected until at the potential E_{ra} (often termed the Flade potential) a little below the passivation potential, reactivation occurs. The reactivated metal dissolves in the normal way up to a dissolution potential, E_d, below which the metal moves towards its immunity area.

* In the present study the term E_t, 'transpassivation potential', will be used for potentials at which the passive current density becomes equal to 1·5 mA cm^{-2}.

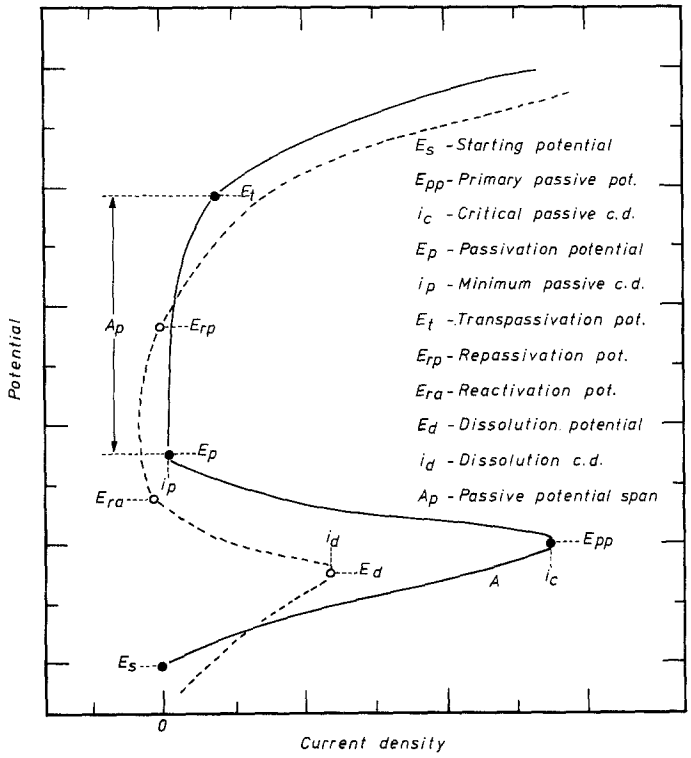

Fig. 3. Diagrammatic representation of an anodic polarization curve for a metal in a molten sulphate-containing environment.

The following points are understood in presentation and discussion of data: (i) Potentials are referred to the standard Ag/Ag^+ electrode; (ii) Current density is calculated using the geometric area; (iii) Dashed lines on polarization curves represent reverse sweeps; (iv) Sodium chloride concentrations are given in wt.%; (v) The equilibrium partial pressures of SO_3, in the experimental system at a total pressure of 1 atm, are given in atmospheres; and (vi) The metal oxides referred to as MO may in fact be solvated forms of these oxides.

3.2. *Results of the anodic behaviour of Ni*

Potentiodynamic anodic polarization curves at 900° C for Ni in molten Na_2SO_4, NaCl, and Na_2SO_4–NaCl mixtures in laboratory air and under 5×10^{-5} atm SO_3 are given in Figs. 4–14. The curves for these corrosion specimens in pure Na_2SO_4 under greater SO_3 atmospheres are given in Fig. 14.

The reproducibility of the curves regarding the potentials such as dissolution, reactivation, passivation, repassivation, transpassivation and starting, was within 50 mV for all runs. Reproduc-

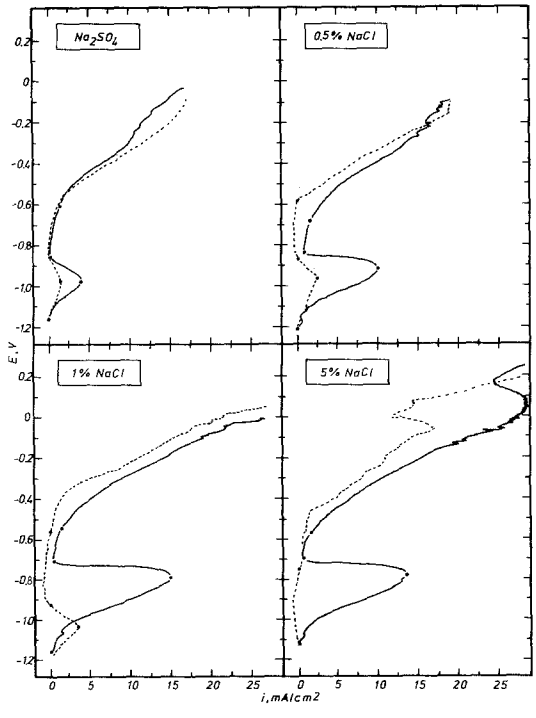

Fig. 4. Potentiodynamic polarization curves for nickel in Na_2SO_4, Na_2SO_4–0·5% NaCl, Na_2SO_4–1% NaCl and Na_2SO_4–5% NaCl at 900° C, in air (first polarization).

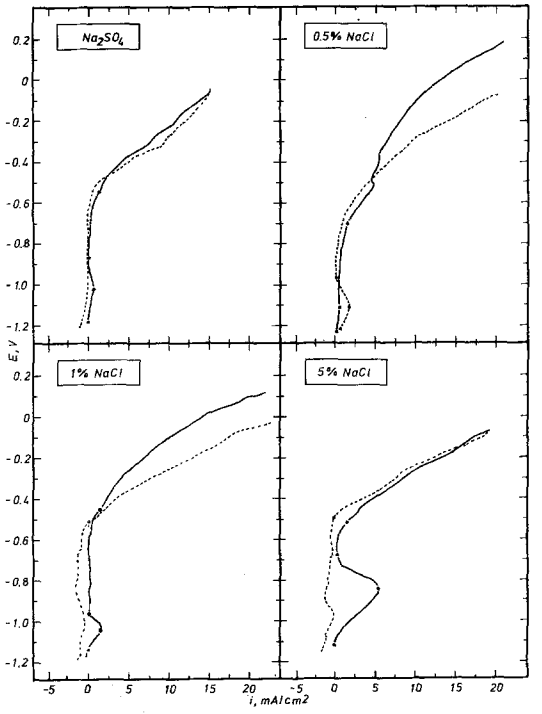

Fig. 5. Potentiodynamic polarization curves for nickel in Na_2SO_4, Na_2SO_4–0·5% NaCl, Na_2SO_4–1% NaCl, and Na_2SO_4–5% NaCl at 900° C, in air (second polarization).

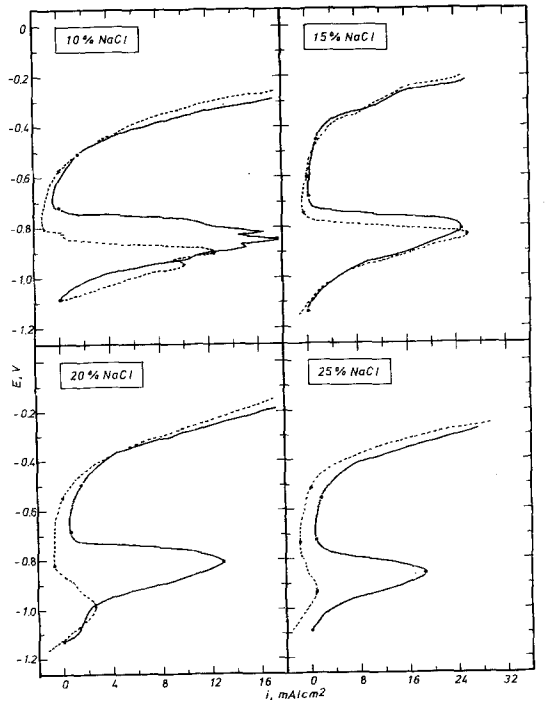

Fig. 6. Potentiodynamic polarization curves for nickel in Na_2SO_4–10% NaCl, Na_2SO_4–15% NaCl, Na_2SO_4–20% NaCl, and Na_2SO_4–25% NaCl at 900° C, in air (first polarization).

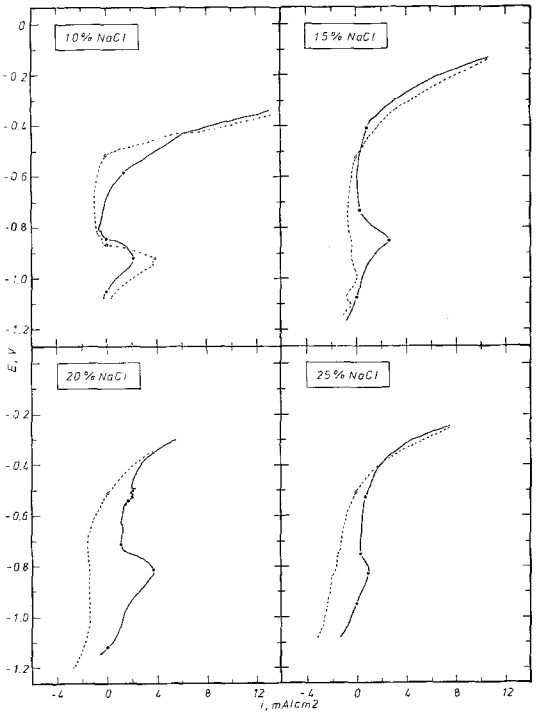

Fig. 7. Potentiodynamic polarization curves for nickel in Na_2SO_4–10% NaCl, Na_2SO_4–15% NaCl, Na_2SO_4–20% NaCl and Na_2SO_4–25% NaCl at 900° C, in air (second polarization).

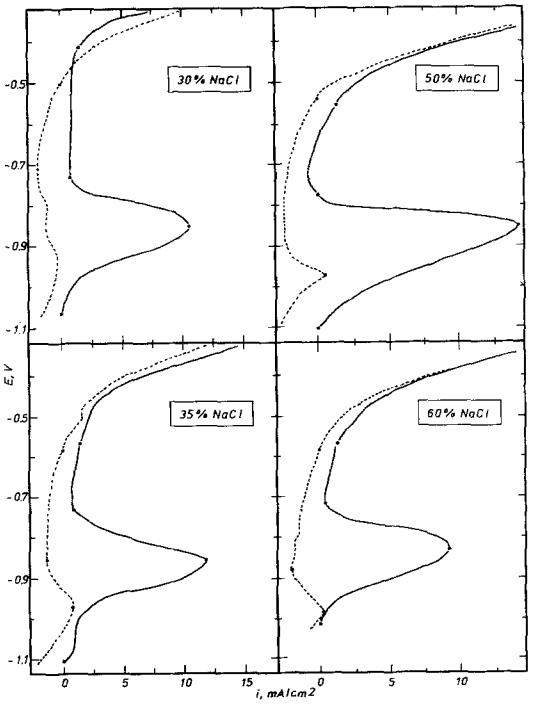

Fig. 8. Potentiodynamic polarization curves for nickel in Na_2SO_4–30% NaCl, Na_2SO_4–35% NaCl, Na_2SO_4–50% NaCl and Na_2SO_4–60% NaCl at 900° C, in air (first polarization).

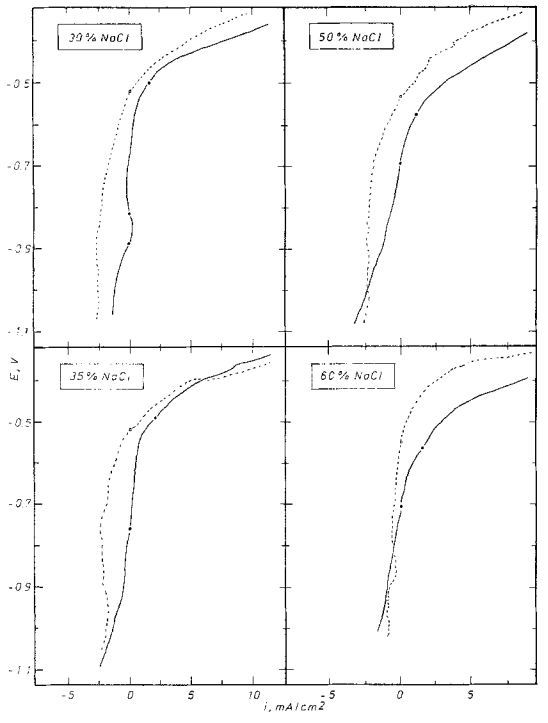

Fig. 9. Potentiodynamic polarization curves for nickel in Na_2SO_4–30% NaCl, Na_2SO_4–35% NaCl, Na_2SO_4–50% NaCl, and Na_2SO_4–60% NaCl at 900° C, in air (second polarization).

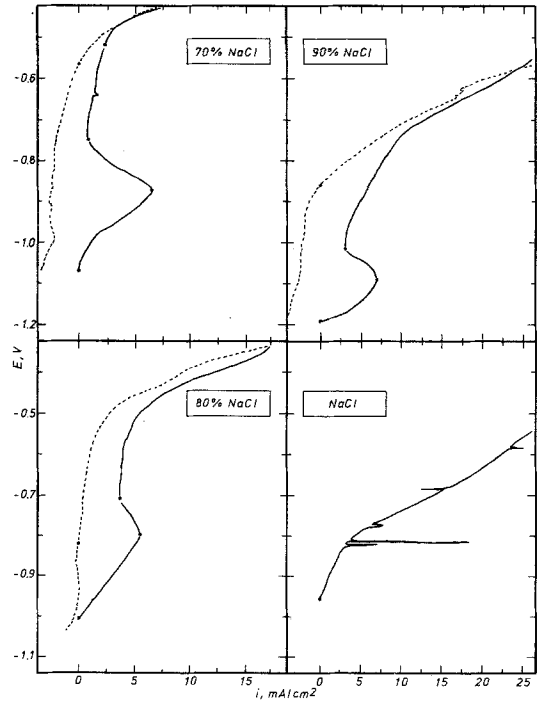

Fig. 10. Potentiodynamic polarization curves for nickel in Na_2SO_4–70% NaCl, Na_2SO_4–80% NaCl, Na_2SO_4–90% NaCl, and NaCl at 900° C, in air (first polarization).

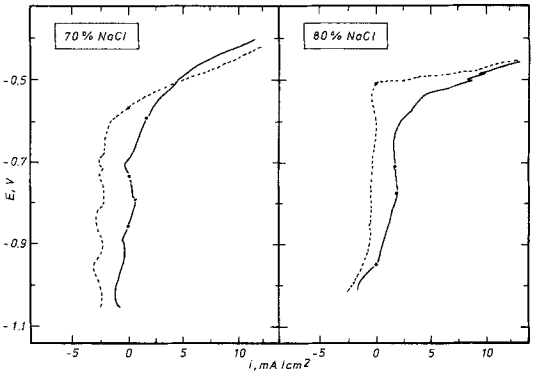

Fig. 11. Potentiodynamic polarization curve for nickel in Na_2SO_4–70% NaCl, and Na_2SO_4–80% NaCl at 900° C, in air (second polarization).

ibility of current densities at the various transition points was within +100% to −30% in all cases.

3.3. *Dissolution and passivation of Ni in Na_2SO_4*

When a mechanically polished nickel electrode contacts molten sodium sulphate at 900° C, in air, the initial electrode potential is about −0·8

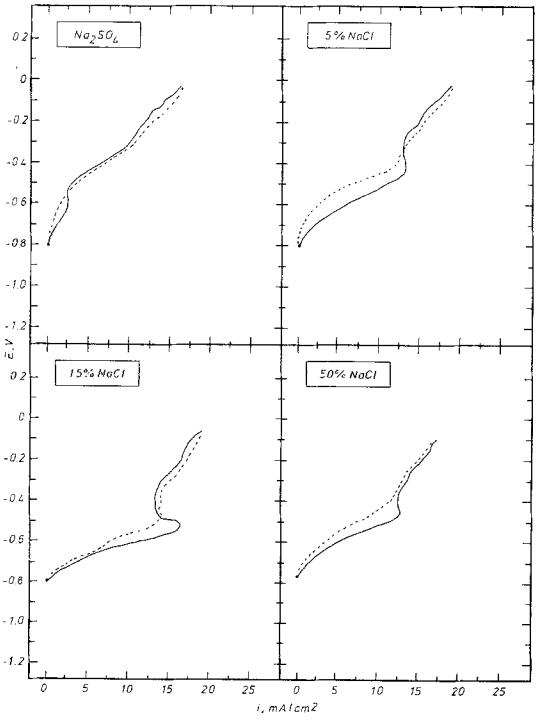

Fig. 12. Potentiodynamic polarization curves for nickel in Na_2SO_4, Na_2SO_4–5% NaCl, Na_2SO_4–15% NaCl, and Na_2SO_4–50% NaCl at 900° C under 1 atm O_2 and 5×10^{-5} atm SO_3 (first polarization).

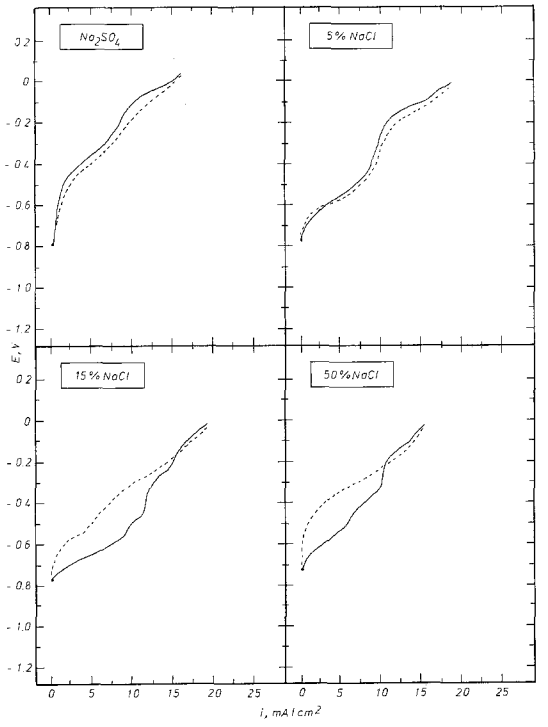

Fig. 13. Potentiodynamic polarization curves for nickel in Na_2SO_4, Na_2SO_4–5% NaCl, Na_2SO_4–15% NaCl, and Na_2SO_4–50% NaCl at 900° C under 1 atm O_2 and 5×10^{-5} atm SO_3 (second polarization).

to −0·9 V and changes rapidly to −1·16 V. If an *E–i* curve is initiated from this immersion potential (which is the starting potential, E_s, in agreement with conventions made above) the current increases continuously up to a maximum value at a certain potential and afterwards a decrease of current down to a minimum value occurs. The maximum current is a critical passive current, i_c, occurring at the primary passive potential of the nickel in the melt, E_{pp} (Fig. 4). The residual current is the minimum passive current, i_p, or the dissolution current of passive nickel. An increase of potential of about 0·35 V beyond E_{pp} produces a relatively small charge in the current. Therefore in the potential region between −1·1 V up to −0·6 V, the *E–i* curve shows a typical onset of passivity on the nickel electrode. Beyond this region an increase of current is observed corresponding to the transpassivity area. In the transpassive area, the change of slope of the *i–E* line at currents beyond 10 mA cm^{-2} suggests the initiation of another transpassive process. Retracing the *E–i* characteristic in the reverse direction, the returning curve now involves a passivated nickel electrode and it exhibits in the passive–active area

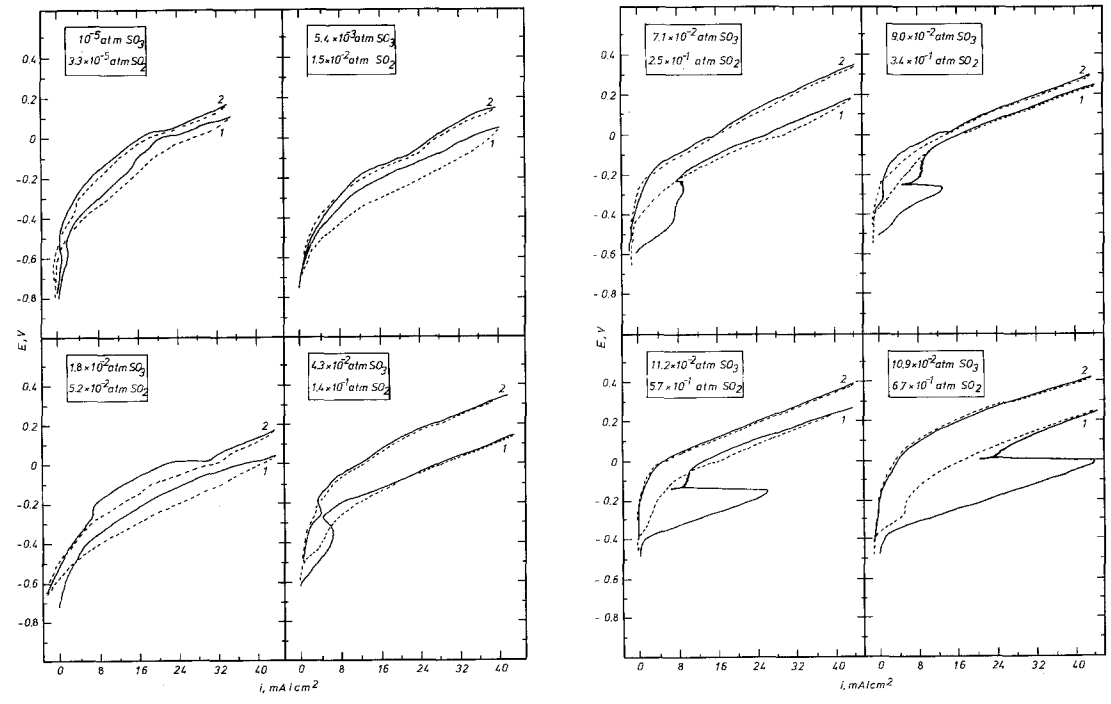

Fig. 14. Effect of SO_3 partial pressure on the potentiodynamic polarization curves for nickel in Na_2SO_4 at 900° C (curves marked 1, first polarization; curves marked 2, second polarization).

Table 1. Polarization characteristics of nickel in molten Na_2SO_4/NaCl salts at 900° C, in air, relative to the first anodic polarization scans (E mV; i mA cm^{-2})

Medium	E_s	E_{pp}	i_c	E_p	i_p	E_t	E_{rp}	E_{ra}	E_d	i_d
Na_2SO_4	−1160	−980	4	−860	0·25	−610			−980	1·5
0·5% NaCl	−1210	−910	10	−840	0·5	−660	−580	−860	−960	2·5
1% NaCl	−1160	−790	15	−710	0·25	−530	−560	−930	−1020	3·25
5% NaCl	−1120	−770	13	−700	0·25	−550	−750			
10% NaCl	−1080	−850	17·3	−720	0	−510	−570	−810	−910	12·3·
15% NaCl	−1130	−820	25	−680	0·33	−455	−600	−740	−835	25·8
20% NaCl	−1130	−810	13	−680	0·50	−505	−550	−830	−960	2·5
25% NaCl	−1090	−860	18·5	−720	0·80	−560	−530	−760	−915	0·8
30% NaCl	−1060	−845	10·8	−730	0·64	−430	−510			
35% NaCl	−1110	−860	11·0	−740	0·70	−560	−580	−860	−970	0·5
50% NaCl	−1110	−840	14	−790	0	−560	−540		−980	0·3
60% NaCl	−1010	−830	9	−710	0·4	−560	−580	−885	−970	0·4
70% NaCl	−1070	−870	7	−750	0·8	−520	−570			
80% NaCl	−1010	−800	5·3	−710	3·4		−820			
90% NaCl	−1190	−1090	6·5	−1020	3·0		−860			
NaCl	−960									

a small loop corresponding to the reactivation of the electrode.

Most of the features mentioned above prevail also in the second polarization. The most marked differences appear in the transpassivation potential, E_t, which is more positive than in the previous case, the critical passive current, i_c, which is very small and not so clearly defined, and the reactivation loop which is not observed (Fig. 5). Parameters deduced from the potentiodynamic E–i curves are assembled in Tables 1 and 2.

Looking at the first potentiodynamic E–i curve, it appears at first sight that the initial portion of the curve, below E_{pp}, corresponds to the dissolution of nickel. This is, however, not true. Free-exposure tests for Ni in pure Na_2SO_4, in air, showed that once a maximum negative potential is established at the Ni–sulphate interface, the electrode potential changes slowly but continuously towards more positive values approaching, after about 10 h, a stable potential of −0·5 V (see Part II, Figs. 7 and 8). It is also worthwhile to

Table 2. Polarization characteristics of nickel in molten Na_2SO_4/NaCl salts at 900° C, in air, relative to the second anodic polarization scans. (E mV; i mA cm^{-2})

Medium	$E_{i=0}$*	E_{pp}	i_c	E_p	i_p	E_t	E_{rp}	E_{ra}	E_d	i_d
Na_2SO_4	−1180	−1000	0·75	−860	0·25	−530				
0.5% NaCl	−1230	−1130	0·5			−710		−960	−1110	1·75
1% NaCl	−1140	−1050	1·5	−980	0·1	−460	−530			
5% NaCl	−1120	−850	5·5	−680	0·25	−520	−500			
10% NaCl	−1060	−930	2·2	−850	0	−595	−530	−880	−930	4·0
15% NaCl	−1070	−850	5·4	−730	0·5	−405	−510			
20% NaCl	−1130	−830	3·5	−730	0·9	−555	−520			
25% NaCl	−965	−840	1·8	−765	0·5	−540	−525			
30% NaCl	−880			−820	0	−500	−520			
35% NaCl	−760				0	−490	−520			
50% NaCl	−685				0	−570	−555			
60% NaCl	−710				0	−560	−550			
70% NaCl	−860	−795	0·7	−740	0	−595	−570			
80% NaCl	−960	−785	2·4	−710	1·6		−510			

* $E_{i=0}$ is the potential at which $i = 0$, in the forward sweep.

notice that during the preliminary tests for the selection of the sweep rate for potentiodynamic experiments it was observed that the E–i curve for the Ni–Na_2SO_4 system obtained at a traverse rate of $8{\cdot}5\,mV\,min^{-1}$ exhibited early initiation of passivity. Both these observations and the topochemical examination of a Ni sample potentiostatically polarized in Na_2SO_4 at a potential below E_{pp} (see Part II, Fig. 29) indicate that the first E–i region corresponds to the simultaneous nickel dissolution and passivation. It is obvious, therefore, that reproducibility of results depends strongly on the time elapsed between immersion of the nickel sample and the initiation of the run.

The dissolution–passivation of Ni might be ascribed to the oxidation effect of SO_3. The active potential observed at the beginning would be attributed to a mixed electrode process described by the reactions

$$Ni = Ni^{2+} + 2e \tag{2}$$

and

$$SO_3 + 2e = SO_2 + O^{2-} \tag{3}$$

the SO_3 species deriving from the dissociation [20]

$$SO_4^{2-} = SO_3 + O^{2-}. \tag{4}$$

A subsequent increase of potential would lead to the dissolution of nickel and the formation of nickel oxide by processes such as

$$SO_3 + Ni = SO_2 + Ni^{2+} + O^{2-} \tag{5}$$

and

$$SO_4^{2-} + Ni = SO_3 + NiO + 2e \tag{6}$$

However, the E–pO^{2-} diagram for Ni in pure Na_2SO_4 at 900° C [21] suggests that the SO_3 reduction does not occur in neutral sulphate melts or occurs only at very negative potentials. Therefore, SO_3 reduction is not likely to be the reaction responsible for the dissolution–passivation of Ni. In view of the fact that these two processes at a Ni surface set in as soon as the Ni is exposed to Na_2SO_4, it is assumed that the same primary step is responsible for both passivation and dissolution

$$Ni + SO_4^{2-} \rightarrow Ni\text{–}SO_3 + 1/2\,O_2 + 2e$$

but that in passivation it is followed by

$$\begin{gathered} Ni\text{–}SO_3 + SO_4^{2-} \rightarrow NiSO_4 + SO_3 + 2e \\ NiSO_4 \rightarrow NiO + SO_3 \end{gathered} \tag{7}$$

while in dissolution it is followed by

$$\begin{gathered} Ni\text{–}SO_3 \rightarrow NiSO_3^{2+} + 2e \\ NiSO_3^{2+} \rightarrow Ni^{2+} + SO_3. \end{gathered} \tag{8}$$

In passivation, addition of one SO_4^{2-} ion is rapidly followed by the addition of a second, while in dissolution the formation of $NiSO_3^{2+}$ and its rapid transformation into Ni^{2+} is the process that determines the reaction rate. The mechanism by which the chemisorption of SO_4^{2-} onto Ni occurs may be considered as a donation of electrons associated with the negative charge of SO_4^{2-}, to the unfilled d-shell of a metallic Ni atom, and possibly the driving force for this adsorption is fairly high, since the electronic donation results in a favourable release of energy.

The occurrence of the observed dissolution must be allowed for, even in the case in which the oxide film is the only thermodynamically stable species (as suggested by [21] for the present case), since its formation rate may be slower than the dissolution rate of the first layers of the oxide film.

Ni passivation will be more and more preponderant as the potential is made more positive, and will be the only process above the passivation potential, E_p.

In the potential region between E_p and E_t, a net dissolution of the passivated nickel takes place. The minimum rate of the anodic dissolution of the passivated nickel is given by i_p, and it probably occurs by means of a rather complex mechanism in which diffusion of metal ions from the underlying metal to the oxide–melt interface via cation vacancies could play an important role, as suggested for the reaction between metal and oxygen [22].

Beyond E_t, corrosion of the passive film takes place and simultaneously sulphate discharge might occur (see Part II, Figs. 32 and 33); this discharge, which involves O_2 evolution, is enhanced at currents larger than about $10\,mA\,cm^{-2}$ resulting in local NiO oxidation to NiO_2^-, which decomposes back to NiO as quickly as it moves away from the O^{2-}-rich interface. Therefore, in the transpassive area the following reactions are likely to occur

$$NiO + SO_4^{2-} \rightarrow NiO\text{–}SO_3 + 1/2\,O_2 + 2e$$
$$NiO\text{–}SO_3 \rightarrow NiO + SO_3 \qquad (9)$$

and

$$NiO + O^{2-} \rightarrow NiO_2^- + e$$
$$NiO + NiO_2^- \rightarrow Ni + NiO + O_2 + e. \qquad (10)$$

3.4. *The effect of NaCl and SO_3 on the anodic behaviour of Ni*

The addition of 0·5% NaCl to the sulphate melt significantly increased the current density recorded in the active region of the anodic polarization curve for Ni in pure Na_2SO_4, and slightly changed the other characteristic parameters of the curve (Figs. 4 and 5). Further additions of NaCl, up to 25%, continued to increase the area under the portion of the curve representing the active potential region (Figs. 4, 5, 6 and 7). Since the area under the polarization curve has the units of electrical power per unit area, it could be concluded that increasing additions of NaCl (up to 25%) to the melt increased the electrical power required for passivation of nickel. Over the melt composition range 30–80% NaCl the current densities recorded in the active region were smaller than those recorded in 15–25% NaCl melts, and the characteristic potentials did not vary too much with composition (Figs. 8, 9, 10 and 11).

All the curves (up to 80% NaCl), except those for Ni in Na_2SO_4–5% NaCl and Na_2SO_4–10% NaCl, are similar to the anodic polarization curve for Ni in pure Na_2SO_4. The curve for Ni–5% NaCl shows the initiation of a secondary transpassive process at potentials beyond 0·1 V; this process must correspond to the enhancement of the Cl_2-production, whose evolution, as suggested by simple thermodynamic considerations, might occur at potentials higher than the sulphate discharge potential. This loop was not observed for the other cases since the sweep was reversed at lower potentials (to avoid current densities higher than 25 mA cm^{-2}, which would completely mask the effect of NaCl). The curve for Ni–10% NaCl shows an unusual feature in the active potential range. The increase in potential from E_s to E_{pp} did not result in a smooth E–i relationship, but at about −0·9 V a small decrease in current occurred. This was, however, followed at a slightly higher potential by a further increase in current to the critical passive current, i_c, at E_{pp}. Another peak occurred immediately beyond E_{pp}, just before the current drop for the definite establishment of metal passivity took place. This pseudo- or pre-passivation, which was also very well revealed by the reverse polarization curve could conceivably result from the competition of the normal tendency of the sample to passivate in pure molten sulphate and the activating effect of the chloride ions. For melts with NaCl percentages beyond 80% only dissolution was displayed (Fig. 10).

Tables 1 and 2 show data obtained in molten Na_2SO_4/NaCl salts at 900° C, in air. In addition, a clearer picture of the variation of the characteristic parameters obtained from the E–i curves can be gained by scanning Figs. 15–17 and Table 3.

The main significant features to be noted from these graphs and the table are:

(a) NaCl additions shift the characteristic potentials in the noble potential direction.
(b) The critical passive current density value, i_c, which indicates the ease of achieving passivity, increases with increasing NaCl content of the

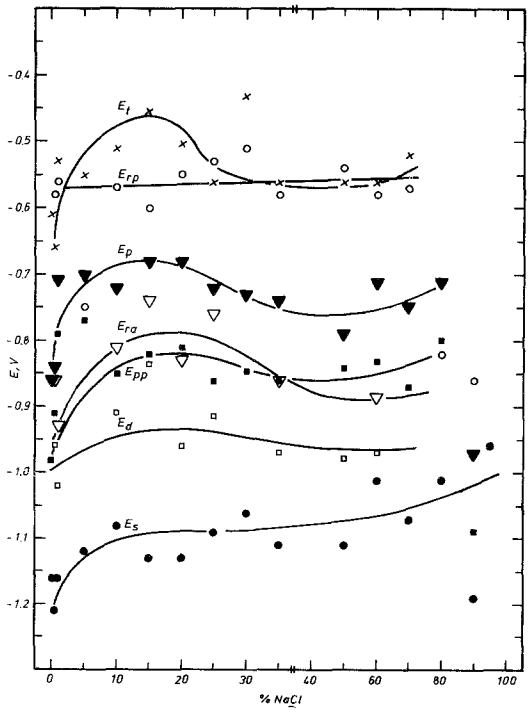

Fig. 15. Characteristic potentials obtained from E–i curves for Ni in molten Na_2SO_4/NaCl salts at 900° C, in air (first polarization).

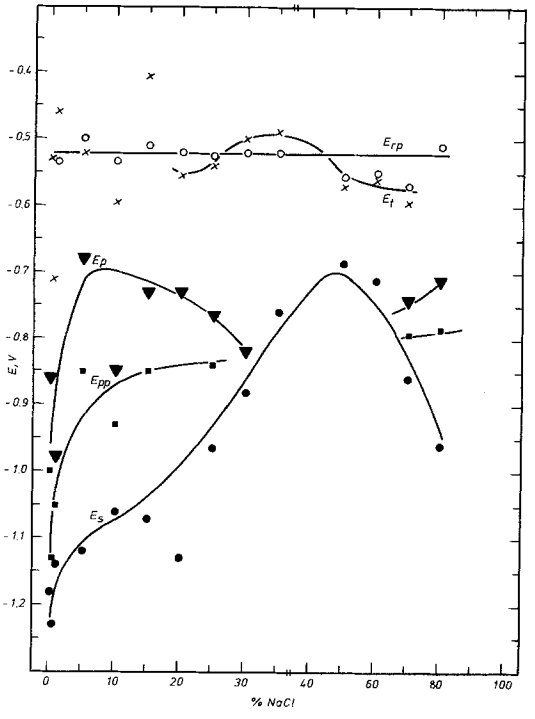

Fig. 16. Characteristic potentials obtained from E–i curves for Ni in molten Na_2SO_4/NaCl salts at 900° C, in air (second polarization).

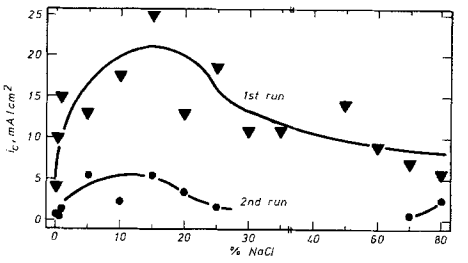

Fig. 17. The effect of chloride concentration on the critical passive current density of Ni anodically polarized in Na_2SO_4/NaCl salts at 900° C, in air.

salt up to a maximum at about 15% NaCl; in general, the dissolution current, i_d, is also much greater on reverse sweeps with Cl^- additions than in plain sulphate.

(c) The potential span in the passive range, A_p, is only slightly decreased by NaCl additions. In addition the ratio A_p/i_p, whose value is experimentally difficult to reproduce, indicates that NaCl has not a significant effect on the extent and stability of the passive region.

From these features, it is concluded that halide additions (especially those up to 25%) affect strongly the anodic behaviour of Ni in the active region and practically do not affect the passive region. Careful analysis of the transpassive part of the polarization curves also showed that the overpassive dissolution current is smaller in Cl^- melts than in SO_4^{2-} alone (see Part II, Fig. 4).

Another two interesting features to note are the constancy of the repassivation potential, E_{rp}, over the melt composition range 0·5–70% NaCl, and the more noble values observed for the starting potential, E_s (shifts towards more negative values

Table 3. Potential span of passive regions and ratios A_p/i_p for Ni in molten Na_2SO_4 plus various concentrations of NaCl

Medium	A_p (mV)		A_p/i_p (mV mA^{-1} cm^2)	
	1st run	*2nd run*	*1st run*	*2nd run*
Na_2SO_4	250	330	1000	1320
0.5% NaCl	180		360	
1% NaCl	180	520	720	5200
5% NaCl	150	160	600	640
10% NaCl	210	255	∞	∞
15% NaCl	225	325	675	650
20% NaCl	175	175	350	195
25% NaCl	160	225	200	450
30% NaCl	300	320	470	∞
35% NaCl	180	270*	260	∞
50% NaCl	230	115*	∞	∞
60% NaCl	150	150*	375	∞
70% NaCl	230	145	290	∞

* In these cases $A_p = E_t - E_{i=0} = 0$.

were only observed with two compositions: 0·5% and 90% NaCl). An explanation for the E_{rp} independence of the NaCl content of the melt is not available at the moment; therefore, the main conclusion derived from this fact is that E_{rp} depends only on the electrode material. One possible reason for the E_s shift to more noble values is that the chloride ion lowers the activity of the oxygen ions within the melt so that its oxidizing ability is rapidly enhanced, consequently minimizing the post-immersion shift towards the maximum active potential, E_s (see Part II, Fig. 7).

Based on the results discussed above, as well as on the information gained from other studies reported in Part II, several successive steps in the Na_2SO_4-induced corrosion process of Ni can be envisaged when NaCl is present initially:

(i) Formation of a Ni_3S_2 layer on the nickel surface, the sulphur required for its formation coming from the dissociation equilibrium reaction existing in sodium sulphate

$$SO_4^{2-} = O^{2-} + 1/2\,S_2 + 3/2\,O_2 \qquad (11)$$

which is displaced to the right by the NaCl addition and by NiO formation.

(ii) Sulphide formation increases the oxide ion activity of the Na_2SO_4 at the Ni_3S_2 scale beneath the salt layer, eventually allowing the dissolution of Ni_3S_2 as $NiCl_2$ or NiO, by reactions of the type

$$Ni_3S_2 + 4NaCl + 1/2\,O_2 = 2NiCl_2 + 2Na_2S + NiO \qquad (K_{900^\circ C} = 1{\cdot}1 \times 10^{-4}) \qquad (12)$$

$$Ni_3S_2 + 3/2\,O_2 = 3NiO + S_2. \qquad (K_{900^\circ C} = 9{\cdot}55 \times 10^{10}) \qquad (13)$$

(iii) As a consequence of this, when an anodic potential is applied to the Ni electrode from its E_s value, dissolution and passivation will occur until the melt becomes saturated with dissolved $NiCl_2$, then preventing further dissolution. It is to be expected that some of the Ni_3S_2 particles (especially the initially very large ones) will grow without intervening in Reactions 12 and 13. Once separated from the melt by the surface layer of the corrosion product they remain stable and can enhance considerably the rate of corrosion of Ni.

(iv) Above E_p and below E_t only passivation of the Ni surface takes place. The film might essentially consist of an outer NiO layer, but inactive adsorbed Cl^--monolayers possibly coexist.

(v) In the transpassive area the behaviour of Ni in melts with or without Cl^- is similar; Cl_2-production is the only process which occurs at the highest potentials, in addition to the NiO corrosion and sulphate discharge observed in Cl^--free melts.

Step (i) explains why E_s for Ni in Cl^--melts is more noble than in sulphate alone. Step (ii) gives account of the higher dissolution rates observed in the active region of the polarization curves for Ni in Na_2SO_4–NaCl melts. This step also gives one possible explanation for the behaviour of the Ni electrodes freely exposed to the salt melts. The more negative values of the free corrosion potentials observed in Cl^--melts might result from Reaction 12 which would no longer be completely stopped, since it is known that evaporation of the $NiCl_2$ from the surface of the melt takes place (see Part II, topochemical observations and analyses). It is also well known that the NiO solubility in Cl^--melts is higher than in sulphate alone.

The maximum rate of attack observed in the active region of the polarization curves for Ni in salt mixtures up to 30% NaCl can either be related to the eutectic in the Na_2SO_4–NaCl system which occurs at 35% NaCl [23], or possibly be associated with the Ni^{2+} critical concentration necessary for the precipitation of the solid product which passivates the metal. The greater fluidity of the eutectic mixture enhances rapid diffusion away from the anode preventing the critical concentration from being exceeded; therefore, maximum i_c values would occur in salt mixtures of around 35% NaCl. The results, however, showed that the maximum i_c occurs at 15% NaCl. One possible explanation is that additions of over 15% NaCl are enough to exceed the solubility product of the passivating solid, thus diminishing i_c in the range 15–30% NaCl. This observation and its possible explanation support mechanism (ii) above and further suggest that Reaction 12 is a critical factor in the Ni passivation.

After studying the effect of NaCl additions on the electrokinetic behaviour of Ni in pure Na_2SO_4, in air, E–i curves were recorded as a function of the SO_3 pressure in contact with the melt. Initially measurements were made by polarizing the Ni electrode immediately after bubbling O_2/SO_2 into the melt. The results were not at all consistent

either with the observation that SO_3 gives rise to a prominent reduction wave in the cathodic polarization curve at an inert Pt electrode in the melt [19] or with the thermodynamic diagram shown in [21] which suggests that, as the acidity level of the melt is raised, more soluble corrosion products are to be expected. On the other hand, the *E–i* curves for Ni in Na_2SO_4 under high SO_3 pressures exhibited immediate initiation of passivity, and the curves in Na_2SO_4–NaCl melts under 5×10^{-5} atm SO_3 approximately followed the curves obtained in air. Since the transport of SO_3 from the gas phase to the metal surface can take place readily in the melt due to the chemical interaction which is represented by the sulphate–pyrosulphate equilibrium

$$SO_3 + SO_4^{2-} = S_2O_7^{2-}$$

the only explanation for the results initially obtained is that a direct interaction of dissolved SO_3 with the melt is absent at beginning. Therefore, the Ni passive behaviour could conceivably result from the oxidizing role of SO_3, giving

$$Ni + SO_3 = NiO + SO_2 \qquad (14)$$

$$(K = 10^6 \text{ at } 900^\circ \text{ C}).$$

If by bubbling SO_2/O_2 mixtures into the melt a direct interaction with SO_3 starts to occur, the acidity of the sulphate anion in terms of the acid–base equilibrium $SO_4^{2-} = SO_3 + O^{2-}$ will be increased, consequently leading to the enhancement of the solubility of the corrosion products, as expected. To check this hypothesis, Ni samples were pre-oxidized in Na_2SO_4 under SO_3 atmospheres, for 3 h, and then subjected to the usual potential sweeps. The *E–i* plots showed a more substantial influence of SO_3, and in addition traces of oxide floating on the surface of the melt were observed. The acidity role of SO_3 on the pre-oxidized Ni may, therefore, be represented by the equation

$$NiO + SO_3 \rightarrow Ni^{2+} + SO_4^{2-} \qquad (15)$$

Based on the conclusions derived above, it was thought that in order to assess the twofold effect of SO_3 on the *E–i* behaviour of Ni it was necessary to bubble SO_2/O_2 into the melts for some time before immersion and polarization of the samples should take place. The *E–i* curves shown in Figs. 12, 13 and 14 were obtained in these conditions

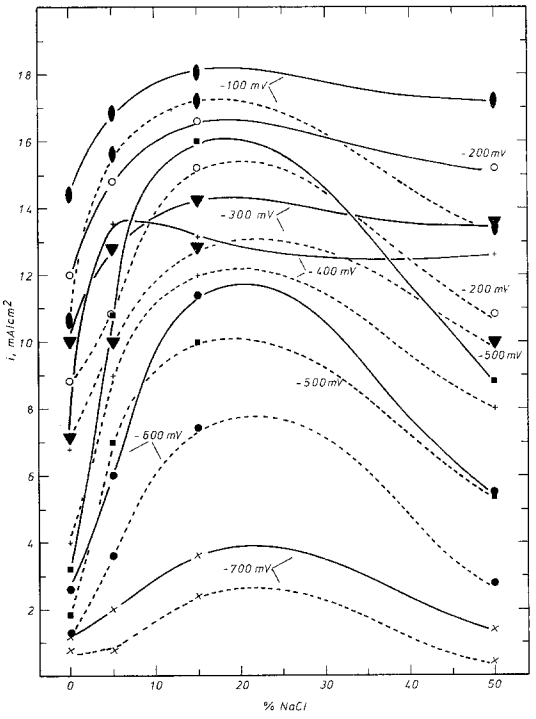

Fig. 18. The effect of chloride concentration on the current density values at the same potential along the anodic polarization curves of Ni in molten Na_2SO_4/NaCl salts at 900° C under 1 atm O_2 and 5×10^{-5} atm SO_3 (full lines, first polarization; broken lines, second polarization).

(see above, electrochemical procedures). From the curves for the melts under 5×10^{-5} atm SO_3 the main conclusions are:

(a) The effect of chloride concentration on the current density values at constant potential is such that the melts in the range 0–25% NaCl are the most aggressive especially in the area of low potentials (Fig. 18).

(b) The fact that the *i* values do not drop even at high potentials, as can be seen in Figs. 12, 13 and 18, shows that the passive capability found for Ni in melts under air is destroyed by SO_3.

(c) Differences between current density values at the same potential, obtained by comparing the polarization curves of Ni in molten Na_2SO_4/NaCl salts in air and under 5×10^{-5} atm SO_3, show [24] that SO_3 has a more substantial influence on the corrosion rates measured in Cl^--melts only and within the potential range −0·7 to −0·3 V, approximately.

The effect of the SO_3 pressure on the *E–i* curves of Ni in molten Na_2SO_4 (Fig. 14) was

investigated by comparing current density at constant overpotential [19]. An increase in SO_3 partial pressure from 1×10^{-5} atm to 7×10^{-2} atm produced only a slight increase in the corrosion rate, but as the SO_3 level was raised relatively high rates were produced especially at low overpotentials. This particular increase of the current densities observed as soon as Ni begins to be polarized may have been due to the immediate formation of soluble corrosion products which are, obviously, likely to form readily at high partial pressures of SO_3. One important point is that the actual increase of the corrosion rates may not result entirely from the SO_3 partial pressure in equilibrium with the melt, but also from the fact that stirring stimulates the cathodic partial reaction(s) which may act as the necessary counterpart to the anodic corrosion reaction. The stirring effect has not been considered in the present work, but there were indications that the corrosion rate is controlled by diffusion [19]; therefore, the high corrosion observed in, say, a 15% NaCl melt under 5×10^{-5} atm SO_3, as compared with the same melt in air, should have been interpreted as the result of two effects; stirring and SO_3 pressure. Present results concerning higher rates of corrosion due to the dissolution stimulating effect of SO_3 may be explained by Equation 5, immediately followed by the unstable intermediate reaction*

$$\mathrm{Ni} + \mathrm{Ni}^{2+} + \mathrm{SO}_4^{2-} \rightarrow \mathrm{NiO} + \mathrm{NiS} + 3/2\,\mathrm{O}_2$$

$$\downarrow + \mathrm{SO}_3$$

$$\mathrm{Ni}^{2+} + \mathrm{SO}_4^{2-}$$

and then

$$\mathrm{NiS} + 3\mathrm{O}^{2-} = \mathrm{Ni}^{2+} + \mathrm{SO}_3 + 8\mathrm{e}. \qquad (16)$$

Reaction 16 would be potential determining at the Ni electrode until Ni^{2+} precipitates, $Ni^{2+} + O^{2-} \rightarrow NiO$, or the conjugate cathodic process $1/2\,O_2 + 2e \rightarrow O^{2-}$ takes place, establishing a rather complex mixed process at the electrode.

3.5. *Dissolution of Ni in molten NaCl*

When Ni exposed to pure molten NaCl at 900° C, in air, begins to be polarized towards more anodic potentials, high current increases are immediately recorded, suggesting that these materials are typically active in the NaCl electrolyte (Fig. 10).

The redox potential of NaCl in air is determined by the reaction equilibrium between oxygen and molten NaCl

$$1/2\,\mathrm{O}_2 + 2\mathrm{Cl}^- = \mathrm{Cl}_2 + \mathrm{O}^{2-} \qquad (17)$$

$$E_{\mathrm{redox}} = E^0_{\mathrm{O}_2/\mathrm{O}^{2-}} + \frac{RT}{2F} \ln \frac{P^{1/2}_{\mathrm{O}_2}}{\{\mathrm{O}^{2-}\}}$$

$$= E^0_{\mathrm{Cl}_2/\mathrm{Cl}^-} + \frac{RT}{F} \ln \frac{P^{1/2}_{\mathrm{Cl}_2}}{\{\mathrm{Cl}^-\}}.$$

Since corrosion of a metal in a given electrolyte is characterized by the redox potential of the latter, the Ni dissolution in the NaCl salt must occur at the expense of the metal interactions with the dissolved oxygen and the chloride ions, as well as with the chlorine and oxide ions formed in the reaction of oxygen with chloride ions [24]. On the basis of the known thermodynamic data for sodium oxide [24] it may be estimated that the concentration of oxide ions and chlorine in molten NaCl at 900° C, in air, is very low; in other words, the rate of Reaction 17 must be very small (but see below) and consequently another simultaneous process should occur to explain the metal corrosion. This accompanying process is probably the reduction of sodium cations, Na^+, to sodium subions, Na_2^+, as has been discussed by Smirnov *et al.* [25]. It is clear that under the influence of polarizing potentials, the rate of these reactions should be significantly high leading to the observed dissolution. It must also be noted that reduction of the Na^+ ions may enhance the kinetics of Reaction 17. For instance, if at the Ni interface dissolution of Ni is initiated by a reaction of the type

$$\mathrm{Ni} + 4\mathrm{Na}^+ \rightarrow \mathrm{Ni}^{2+} + 2\mathrm{Na}_2^+$$

these Ni^{2+} ions may react with O^{2-} ions to form a monoxide deposit beneath the NaCl melt. Removal of O^{2-} ions by this formation shifts the reaction equilibrium 17 to the right hand side, and consequently increases the chlorine dissolved in the melt. The evolved chlorine oxidizes nickel to the dichloride, which in turn may either interact with the O^{2-} ions or diffuse to the melt–air interface where it evaporates.

It is obvious that the direct interaction of dissolved oxygen with Ni resulting in the formation

* The region of stability of NiO does not overlap the stability region of NiS [21] and probably NiO is immediately removed by reaction with SO_3.

of NiO may also be included with, in this case, corrosion proceeding by cracking and failure of the NiO. Once NiO is broken, the reaction $Ni + 2Cl^- \rightarrow NiCl_2$ (volatile) may be the cause of corrosion.

Reactions like the above were substantiated by several topochemical studies (see Part II) and are in agreement with results obtained by Stepanov and Kachina-Pullo [26] in a study of corrosion of steels and nickel in fused KCl and $MgCl_2$ at 800° and 850° C.

Acknowledgements

This work has been carried out with the support of Procurement Executive, Ministry of Defence, UK, and the authors acknowledge some useful discussions with Mr J. F. G. Condé and Mr G. C. Booth of that organization. One of use (C. A. C. S.) is also grateful to Instituto de Alta Cultura (Lisbon) for a bursary.

References

[1] J. F. G. Condé, *J. R. N. S. S.* **28** (1972) 54.
[2] A. J. Arvia, J. J. Podesta and R. C. V. Piatti, *Electrochim. Acta* **16** (1971) 1797.
[3] A. J. Arvia, J. J. Podesta and R. C. V. Piatti, *ibid.* **17** (1972) 33.
[4] G. Baudo, A. Tamba and G. Bombara, *Corrosion–NACE* **26** (1970) 193.
[5] R. G. Casino, J. J. Podesta and A. J. Arvia, *Electrochim. Acta* **16** (1971) 121.
[6] G. N. Kazantsev, I. F. Nichkov and S. P. Raspopin, *Soviet Electrochem.* **2** (1968) 466.
[7] S. Pizzini and L. Agace, *Corrosion Sci.* **5** (1965) 193.
[8] F. Mansfield, N. E. Paton and W. M. Robertson, *Met. Trans* **4** (1973) 321.
[9] W. L. Wheatfall, H. Doering and G. J. Danek, 'Hot Corrosion Problems associated with Gas Turbines', ASTM STP 421, Am. Soc. Testing Mats. (1967) p. 206.
[10] N. D. Greene, *Corrosion–NACE* **18** (1962) 136t.
[11] M. Stern, *J. Electrochem. Soc.* **106** (1959) 376.
[12] N. D. Greene and R. B. Leonard, *Electrochim. Acta* **9** (1964) 45.
[13] A. J. B. Cutler, A. B. Hart, M. J. Fountain and N. H. Holland, ASME Publication No. 67–WA/CD–4 (1967).
[14] L. Greenburgh and M. B. Jacobs, *Ind. and Eng. Chem.* **48** (1956) 1517.
[15] M. G. Hocking, Ph.D. Thesis, University of London (1962).
[16] A. J. B. Cutler, *J. Appl. Electrochem.* **1** (1971) 19.
[17] G. Charlot and B. Tremillon, 'Chemical Reactions In Solvents and Molten Salts', Gauthier–Villars, Paris (1960) p. 539.
[18] H. J. Gardner, C. T. Brown and G. J. Janz, *J. Phys. Chem.* **60** (1956) 1458.
[19] C. A. C. Sequeira, Ph.D. Thesis, University of London (1974).
[20] B. W. Burrows and G. J. Hills, *ibid.* **15** (1970) 445.
[21] C. A. C. Sequeira and M. G. Hocking, *Brit. Corros. J.* (in press).
[22] D. W. Bridges and W. M. Fassell, *Oxidation of Metals* **1** (1969) 279.
[23] G. J. Danek, *Naval Engineers J.* 77 (1965) 859.
[24] A. F. Alabyshev, K. Ya. Grachev, S. A. Zaretskii and N. F. Lantratov, 'Sodium and Potassium', Goskhimizdat, Leningrad (1959).
[25] M. V. Smirnov, V. P. Volodin and I. N. Ozeryanaya, *Dokl. Akad. Nauk SSSR* **155** (1964) 418.
[26] S. I. Stepanov and E. B. Kachina-Pullo, *Zh. Prikl. Khim.* **37** (1964) 379.